AFRL-RW-EG-TR-2018-098

Surface and Interfacial Influences on the Bulk Responses of Composite Materials – AFOSR Annual Report FY2017

Stacy M. Manni
Tomislav Kosta
Jesus Mares Jr.
Steven Pemberton
David B. Hardin

Air Force Research Laboratory
Munitions Directorate/Ordnance Division
Energetic Materials Branch (AFRL/RWME)
Eglin AFB, FL 32542-5910

February 2019

Interim Report

AIR FORCE RESEARCH LABORATORY
MUNITIONS DIRECTORATE

■ Air Force Materiel Command ■ United States Air Force ■ Eglin Air Force Base, FL 32542

This page intentionally left blank

NOTICE AND SIGNATURE PAGE

Using Government drawings, specifications, or other data included in this document for any purpose other than Government procurement does not in any way obligate the U.S. Government. The fact that the Government formulated or supplied the drawings, specifications, or other data does not license the holder or any other person or corporation; or convey any rights or permission to manufacture, use, or sell any patented invention that may relate to them.

Qualified requestors may obtain copies of this report from the Defense Technical Information Center (DTIC) (http://www.dtic.mil).

AFRL-RW-EG-TR-2018-098 HAS BEEN REVIEWED AND IS APPROVED FOR PUBLICATION IN ACCORDANCE WITH ASSIGNED DISTRIBUTION STATEMENT.

FOR THE DIRECTOR:

==Original Signed==	*==Original Signed==*	*==Original Signed==*
JOHN D. CORLEY, PhD	C MICHAEL LINDSAY, PhD	LINDSEY CROMWELL
Ordnance Sciences Core	Technical Advisor	Project Manager
Technical Competency Lead	Energetic Materials Branch	Energetic Materials Branch
Ordnance Division		

This report is published in the interest of scientific and technical information exchange, and its publication does not constitute the Government’s approval or disapproval of its ideas or findings.

This page intentionally left blank

REPORT DOCUMENTATION PAGE

Form Approved
OMB No. 0704-0188

1. REPORT DATE *(DD-MM-YYYY)*	2. REPORT TYPE	3. DATES COVERED *(From - To)*
28 February 2019	Interim	1 October 2016 – 30 September 2017

4. TITLE AND SUBTITLE
Surface and Interfacial Influences on the Bulk Mechanical Responses of Composite Materials – AFOSR Annual Report FY2017

5a. CONTRACT NUMBER

5b. GRANT NUMBER

5c. PROGRAM ELEMENT NUMBER
61102F

6. AUTHOR(S)
Stacy M. Manni, Tomislav Kosta, Jesus Mares Jr., Steven Pemberton, David B. Hardin

5d. PROJECT NUMBER
3002ME71

5e. TASK NUMBER

5f. WORK UNIT NUMBER
W14P

7. PERFORMING ORGANIZATION NAME(S) AND ADDRESS(ES)
Air Force Research Laboratory
Munitions Directorate
Ordnance Division
AFRL/RWME
Eglin AFB FL 32542-5910

8. PERFORMING ORGANIZATION REPORT NUMBER
AFRL-RW-EG-TR-2018-098

9. SPONSORING / MONITORING AGENCY NAME(S) AND ADDRESS(ES)
Air Force Research Laboratory, Munitions Directorate
Ordnance Division
Energetic Materials Branch (AFRL/RWME)
Eglin AFB FL 32542-5910
Technical Advisor: C. Michael Lindsay, PhD

10. SPONSOR/MONITOR'S ACRONYM(S)
AFRL-RW-EG

11. SPONSOR/MONITOR'S REPORT NUMBER(S)
AFRL-RW-EG-TR-2018-098

12. DISTRIBUTION / AVAILABILITY STATEMENT
Distribution A: Approved for public release; distribution unlimited. Approval Confirmation 96W-2019-0046 dated 20 February 2019

13. SUPPLEMENTARY NOTES

14. ABSTRACT
This report details the initial results for an effort investigating the relationship between a material's chemical and physical properties. Sylgard 184 and hollow glass beads of various sizes have been selected as the system of interest. Characterization methods are in development, including room temperature inverse gas chromatography of polymer composites, stress and strain curves of single bead inclusion with digital image correlation, and standard surface and mechanical testing methods. Additional research and results are included in the year two and final reports for this effort.

15. SUBJECT TERMS
surface and interfacial energy, stress and strain measurements, digital image correlation, inverse gas chromatography, Sylgard 184 and glass beads, surface and mechanical property relationship

16. SECURITY CLASSIFICATION OF:			17. LIMITATION OF ABSTRACT	18. NUMBER OF PAGES	19a. NAME OF RESPONSIBLE PERSON
a. REPORT	b. ABSTRACT	c. THIS PAGE			Lindsey Cromwell
UNCLASSIFIED	UNCLASSIFIED	UNCLASSIFIED	SAR	36	19b. TELEPHONE NUMBER *(include area code)*

Standard Form 298 (Rev. 8-98)
Prescribed by ANSI Std. Z39.18

This page intentionally left blank

ANNUAL LABORATORY TASK REPORT

LRIR #: 17RWCOR469

Title: Surface and Interfacial Influences on the Bulk Mechanical Responses of Composite Materials

Reporting Period: 1 Oct 2016-30 Sep 2017

Laboratory Task Manager: Stacy M. Manni, AFRL/RWME

Commercial Phone: 850-882-0357 **DSN:** 872-0357

Mailing Address: AFRL/RWME
Dr. Stacy M. Manni
2306 Perimeter Rd
Eglin AFB, FL 32542-5910

Email Address: stacy.manni@us.af.mil

AFOSR Program Manager: Dr. Martin Schmidt

Research Overview:

This research effort is investigating the surfaces and interfaces in heterogeneous energetic formulations and discovering the effects these regions have on the bulk properties of energetic materials (EM), quantifying these effects on mechanical properties and accounting for these effects in the model and design of new materials. This is being accomplished by developing characterization techniques (task 1) capable of elucidating the surface and interfacial properties of EM conglomerates. These materials are also being characterized using a suite of mechanical properties testing (task 2) modified specifically for these materials. These steps are being repeated with a host of incrementally different materials then increasingly complex materials. Data obtained from characterization and testing are being correlated (task 3) to distinguish potential relationships between surface and interfacial properties and bulk mechanical properties. Information from this study and a related AFOSR microstructure LRIR are being combined to develop unit cells that describe the types of interactions seen in EM, and will finally be incorporated into existing programs to account for surface and interfacial effects in modeling and simulation efforts (task 3) for future EM formulation efforts.[1] At the conclusion of this research effort we will have gained a qualitative and quantitative understanding of the role interfaces play in EM composites and will have a mathematical framework that will aide in creating novel EM formulations with application-driven and tailored mechanical properties.

Figure 1. Image highlighting the meso-structures present in a filled high explosive munition. There are a number of interfacial characteristics including boundaries and/or intermixing between the main fill material, liner material and case material.

Surfaces and interfacial characteristics and their effects on standard performance metrics, such as mechanical properties, have increasingly become topics of conversation within the energetic materials community. It is critical to understand these effects in heterogeneous composites as they directly affect a material's agglomeration behavior, process induced disorder, work of cohesion/adhesion, surface chemistry and charging, wettability of surfaces, and powder mixing, flow and segregation. On the macroscale, Figure 1, these features are often the locations of mechanical failures, interesting chemistry, and void formation and contribution to initiation and detonation physics. On the microscale, Figure 2, surfaces and interfaces are the dominant feature of the system. It is clear that there is a need and desire to better understand these features, yet very little is known about them and their role in influencing bulk characteristics. This gap in knowledge is closing as new techniques are discovered that are capable of probing these regions but there remains numerous questions about what surface and interfacial properties are most beneficial to characterize for a given system, how these regions affect bulk properties, and how surface and interfacial properties can be reliably related to historically measured bulk properties and performance characteristics without having to make and test each formulation iteration individually.

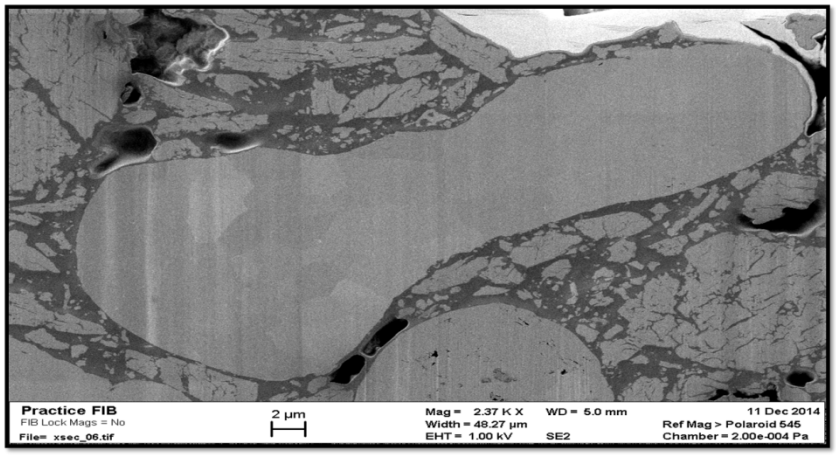

Figure 2. SEM image of an inert simulant energetic formulation. This image shows the various types of surfaces and interfaces present in this heterogeneous composite (composed of 3 different types of particulates, a polymeric binder, various additives and voids).

The Air Force (AF) requires munitions items capable of surviving increasingly stressful environments; such as high temperature or pressure. Harsher environments will continue to be a challenge as targets become harder and more deeply buried. Compression during penetration events can lead to premature detonation, or to detonation failure if delamination occurs at the Fuze interface and the material stretches away from the Fuze. All materials undergo some degree of ageing during their life cycle. Thermal cycling and ageing can lead to a number of surface and interfacial issues such as delamination and the creation of voids. Ageing can be problematic both on the macroscale and on the microscale. These locations become points for potential material failure and preignition. Voids can be particularly troublesome as they can become hot spots and lead to unintentional initiation points. It is very likely that material interfaces and surfaces also have implications in the overall and inherent sensitivity and safety of energetic materials. Understanding the effects surfaces and interfaces have on an energetic material's bulk characteristics is paramount to being able to remain agile in the face of tomorrow's warfighting needs.

It is unknown how the chemistry of the interface (on the micro- or macroscale) affects the strength of the interface or how both affect the bulk properties of current energetic material formulations. This area of research is ripe for discovery and innovation. Once a basic understanding is obtained, it will be possible to explore modification of surfaces and interfaces in order to design materials with more desirable bulk properties. Moving forward, there is a need for resilient materials as tomorrow's warfighting needs are unknown. Obtaining a fundamental understanding of interfacial features and their performance effects will enable DoD and DOE scientists and engineers to meet those future needs.

A Note on Funding and Timing

Funds for this effort arrived on May 10, 2017. Due to funding not arriving until the 8th month of the fiscal year, it was impossible to meet all year one goals and objectives. As a result this report does not contain a great deal of data, analysis or information about the project. Once the project reaches the goals and objectives for year one, an interim technical report will be generated containing all of the data and analysis that would have been contained in this report had funding not been delayed by continuing resolutions.

Technical Summary of FY17 Progress:

1 Surface and Interfacial Characterization

1.1 Surface and Interfacial Characterization Goals and Objectives

The purpose of task 1 of this research effort is to broaden the general understanding of the properties and characteristics of surface and interfacial regions within heterogeneous mixtures. In order to meet task goals, the following objectives are being addressed. A flexible methodology is being developed based upon existing inverse gas chromatographic (IGC) methods that is capable of providing surface and interfacial properties of a diverse range of materials; particularly glass beads and silicone binder systems. Properties of interest include surface energies (dispersive and specific), works of adhesion and acid/base character. Once the methodology is firmly established, there will be a systematic build-up from homogeneous particulate materials (Sylgard 184 silicone binder system and hollow glass beads of a single particle distribution) to other two-component simple systems (other binder systems) and then to multi-component heterogeneous mixtures of increasing complexity. Through observation of the systematic differences between a single component material and the more complex mixture, a more thorough understanding of the effects of each individual component on the overall heterogeneous mixture can be elucidated. This task will produce a series of materials (single to multi-component) with well characterized surface and interfacial properties which can then be studied for their effects on bulk mechanical properties of interest (including relationships and correlations) and for inclusion into current modeling and simulation efforts.

Major technical challenges include (1) sample preparation methods - exposure of surface and interfacial regions of interest in samples, (2) ensuring IGC measurements are of the surface and not bulk properties and (3) relating the surface and interfacial properties of a raw or simplistic material to those of the more complex system. These challenges are being addressed through (1) exploration of a number of sample preparation techniques including columns and thin films, studying the differences between as-cured surfaces exposed to different environments (air, nitrogen or Teflon), mechanical exposure of the interior of a sample (scalpel, microtome, etc.) vs. the exterior of a sample, and comparison of IGC findings to standard contact angle goniometer measurements as found in literature. Some materials interact with the probe molecules so strongly that they enter the material bulk and can interfere with other probe molecule retention times or provide characteristics of the bulk instead of the surface. This can be overcome by (2) closely monitoring signal/ time curves for signs of strong interactions, adjusting temperature, flow rate, probe concentration and at times eliminating particularly troublesome probe molecules.

1.2 Material Preparation

Initial material preparation looked at a number of binder systems of interest. A clear, two-part binder system was preferred for mechanical analysis of interfaces about particles. Hydroxyl-terminated polybutadiene binder, Epoxy and polydimethylsiloxane (PDMS) were all considered. PDMS, commercially available as Sylgard 184, was selected as the preliminary material due to its cost effectiveness, easy mixing/casting properties and short cure times. Sylgard 184 is composed of a 10:1 mixture of resin to curative and produces a reliable and repeatable casting and cure. Additional attractive features of Sylgard 184 are that laboratory scale samples can cure overnight at room temperature or on the order of a few hours at elevated temperatures (~60-100 °C), sample

preparation does not involves hazardous isocyanates, unlike the HTPBs and resulting material is more flexible than its epoxy counterparts (preferable for an initial study).

For the filler phase, we considered beads of various compositions (glass, various metals and polymer). All solid samples had void, settling and density issues at all particle sizes. Void issues were addressed through heat treatment. Settling and density issues were not able to be overcome through any temperature or mechanical means using the chosen polymer matrix. For this reason, glass beads were chosen because they are both cost effective and readily available in low density, high strength, hollow forms. 3M hollow glass beads were chosen exclusively because they were within our budget and time constraints. The particle sizes are severely limited (under 75 µm) and we will need to identify alternate particulates (likely polymer based depending on viscosity and cure rate of the binder system) for future sample series. Using Sylgard 184 and 3M hollow glass beads (20 µm or 60 µm), density was confirmed to be consistent for all sample configurations used in this study; including standard dogbones, thin/thick films, pucks, and other molded samples. Maximum hollow glass bead volume percentage, while retaining consistent, workable sample properties, was 45%. Sylgard 184 and 3M hollow glass bead (20 µm or 60 µm particle sizes at 80% pore size distribution) samples within this study contain 5%, 15%, 25%, 35% or 45% glass beads by volume.

1.3 Method development and preliminary results

IGC allows numerous surface phenomena to be quantified to include the total surface energy (γ_s), dispersive surface energy component (γ_s^d), specific surface energy component (γ_s^{sp}), work of cohesion and adhesion (W_C, W_A), heats of sorption (ΔH), acid or base constants (K_a *or* K_b), partial solvation parameters based on quantum mechanical analysis, Hildebrandt solubility parameter, crosslink density, diffusion coefficient, chemisorption and physisorption affinity and specific surface area (SA_{BET}) determinations from adsorption and desorption isotherms.[2-11] Bulk properties which can be determined from IGC include the glass transition temperature (T_g), solubility parameter, polymer cross-linking and diffusion coefficient.[11]

This task will utilize IGC to develop a methodology capable of measuring surface and interfacial properties for a wide variety of sample types. IGC is a chromatography technique in which the material to be investigated is present as the stationary phase and small quantities of well understood probe molecules in an inert carrier gas (He) are used as the mobile phase; probe molecules include a series of non-polar alkanes (hexane, heptane, octane, nonane, decane and undecane) and polar molecules (acetone, tetrahydrofuran, ethyl acetate, acetonitrile, chloroform).[12] At infinite dilution, adsorption of probe molecules is independent of the surface coverage, does not include lateral interactions of probe molecules and results in a linear isotherm described by Henry's Law. This experimental mode probes the highest energy sites on a material's surface.[13] Retention times from the resulting Gaussian peak maximums are used to calculate retention volume, V_N, by:[3]

$$V_N = \frac{j}{m} F(t_R - t_0) \frac{T}{273.15K} \quad (1)$$

Where j is the James-Martin compression correction factor, m is the sample mass, F is the exit flow rate at 1 atm and 273.15 K, t_R is the retention time of the adsorbing probe from the peak max, t_0 is the dead time as determined from methane, and T is the column temperature in K. The greater the value of V_N, the greater the affinity of the probe molecule for the investigated material's surface. The dispersive surface energy, γ_s^d, can be found experimentally by injection of a series of

alkane probe molecules and finding the slope of a plot of $RT\ ln\ V_N$ vs. $a\ \gamma_L^d$, according to the following equation:[3, 14-15]

$$RT \ln V_N = 2N_A (\gamma_s^d)^{1/2}\ a\ \left(\gamma_L^d\right)^{1/2} + constant \quad (2)$$

Where R is the gas constant, N_A is Avogadro's number, a is the cross sectional area of the probe molecule and γ_L^d is the surface tension of the probe molecule. The specific surface energy (polar component), γ_s^{sp}, can be found by adding polar probe injections to the above plot and measuring their distance from the straight line formed by the alkane probes. The difference found is equivalent to the specific component of the free energy of desorption, ΔG_{sp}, according to:[3]

$$\Delta G_{sp} = RT \ln V_N - RT \ln V_N^{ref} \quad (3)$$

The specific surface energy can also be found by exploration of the acidity and basicity of a material using acidic and basic polar probes through the van Oss concept: [4, 27-28]

$$\Delta G_{sp} = 2\ N_A\ a_m\ \left((\gamma_L^+\ \gamma_s^-)^{1/2} + (\gamma_s^+\ \gamma_L^-)^{1/2}\right) \quad (4)$$

Where a_m is the surface coverage, γ_s^+ and γ_s^- are the acid and base parameters for the surface and γ_L^+ and γ_L^- are the electron acceptor and donor parameters of the probe molecule. Once the acid and base parameters are understood, the specific surface coverage can then be obtained by:[4, 17-19]

$$\gamma_s^{sp} = 2\ (\gamma_s^+\ \gamma_s^-)^{1/2} \quad (5)$$

Adsorbate (material a) and substrate (material b) interactions and interfacial shear strength can then be calculated using the dispersive surface energies and acid base parameters for the materials. Work of adhesion, W_A, can be derived by:[20, 21-22]

$$W_A = 2\left(\gamma_a^d\ \gamma_b^d\right)^{1/2} + 2\ (\gamma_a^+\ \gamma_b^-)^{1/2} + 2\ (\gamma_b^+\ \gamma_a^-)^{1/2} \quad (6)$$

Up until this point, all experiments and calculations described occur within the infinite dilution regime (10^{-3} to 1 mg probe molecules).[23] Infinite dilution experiments take place within the Henry's Law region of the adsorption isotherm and probe the most highly energetic sites in a material which allows for very high sensitivity. Measurements at infinite concentration provide complimentary information as probe molecules interact with all sites on the surface.[13] By investigating materials in this regime, lower surface energy sites and concentration of sites at each energy level can be probed and results are more comparable to the average surface energy measurements found in contact angle goniometry (CAG). Surface energy heterogeneity in a material is an important property in understanding the energy across an entire material. As previously discussed, injection of a series of alkane and polar probe molecules at the same molar concentration (surface coverage) can give both the dispersive and specific surface energies at that surface coverage. Repetition over a range of probe molecule concentrations (finite concentration) gives a surface energy profile for a material (a distribution of surface energies as a function of surface coverages). Integration of each point of the profile and plotting surface energy (γ_s^d or γ_s^{sp}) vs. percentage of surface coverage will give surface energy distributions which allow for evaluation and comparison of surface energy heterogeneity.[14, 17, 19, 24-25]

The current set-up at RWME utilizes a refrigerating incubator system separate from the IGC system that provides for greater temperature control (down to 5 °C from 35 °C), makes use of a thin film cell (easier sample preparation but the longer column length has repercussions on resolution) and has allowed for the surface property measurements of challenging samples with very strong interactions with probe molecules.

Method development for the samples in this study is nearly complete with the major complications being extremely low retention of the probe molecules, Figure 3, and the instrument software not being able to account for the glass beads being hollow. The low retention is being addressed primarily through temperature, flow rate and sample size control and the software limitation is being addressed through manual data analysis. Analysis of samples by IGC should be completed within 2 months.

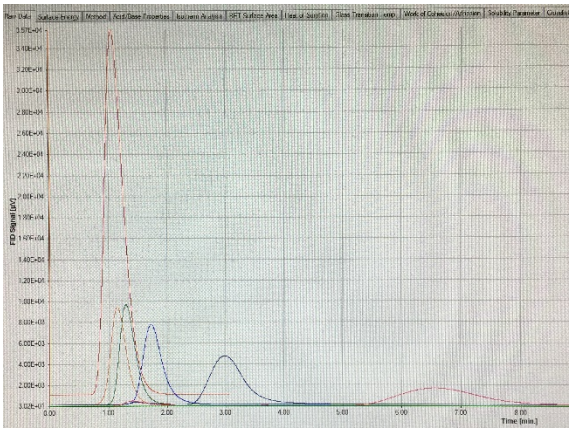

Figure 3. IGC Analysis of preliminary Sylgard 184 and hollow glass bead samples (20) to demonstrate analysis methodology. Nonpolar probe molecules (methane-red, hexane-orange, heptane-green, octane-blue, nonane-violet, decane-pink) are well resolved, symmetrical, and elute within a reasonable amount of time.

1.4 Plans for FY18

Research plans for FY18 Surface and Interfacial Chemical Properties Characterization include:

- Method development with Sylgard 184 and 3M hollow glass beads will be completed;
- Samples from the preliminary study (Sylgard 184 and 3M hollow glass beads of 2 particle sizes – 20 µm and 60 µm) will be analyzed via IGC using method currently under development;
- Depending upon analysis and modeling of Sylgard 184 and 3M hollow glass beads, a more complex set of samples will be developed and tested to add to the newly developed correlation (material preparation, IGC method development and IGC analysis);
- Analysis approval for energetic particulates by IGC will take place in order to study more complex energetic systems;

- Crosslinking density will be added as parameter of study (IGC, FTIR and DMA determinations) due to collaborative effort with AFRL/RQ.

2 Mechanical Properties Studies

2.1 Mechanical Characterization Overview

The goal of the mechanical characterization task is to measure interface debonding strength in polymer bonded explosives. This feeds into the overall goal of the Laboratory Task of correlating interfacial mechanical properties with interfacial chemistry by providing deterministic and stochastic measurements of interface debonding strength.

In this work, measurement of interface debonding strength is accomplished in two ways – implicitly and explicitly. In the implicit approach, bulk properties measured on a family of hyper engineered composites where composition variables such as filler volume fraction, filler particle size, filler particle surface chemistry, etc. are well-controlled and characterized and then constructing correlations between bulk properties and composition details. With the implicit approach, we hope to elucidate the effect of surface chemistry on particle-binder interface strength as well as the effect of particle-binder interface strength on bulk composite properties. In the explicit approach, we will attempt to directly measure particle-binder interface strength by way of targeted mechanical experiments which control the stress and strain state such that the mechanical load at an interface can be directly quantified. This report summarizes the to-date experimental data for the implicit approach.

2.2 Mechanical characterization methodology

Mechanical characterization of the composites was accomplished using the Instron 5982 screw-driven uniaxial tension/compression load frame at AFRL/RWME, shown in 4, below.

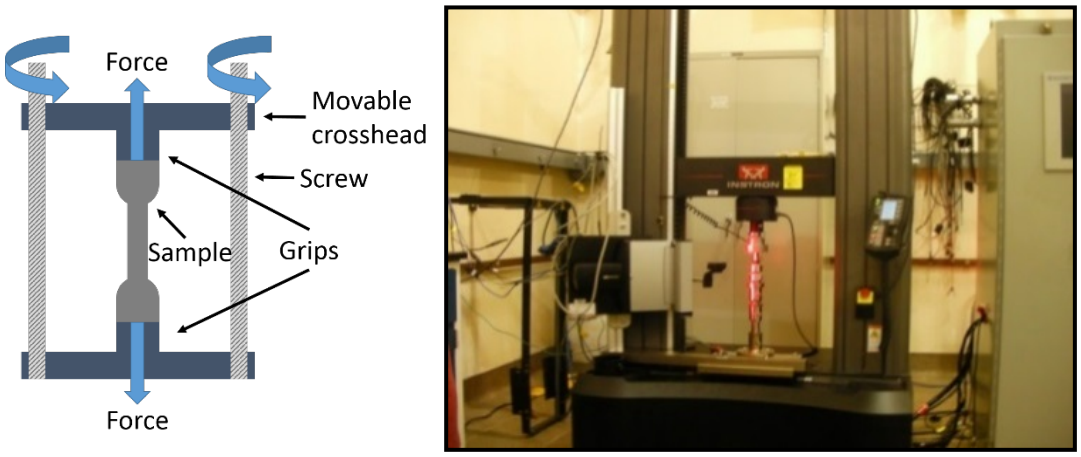

Figure 4. Schematic of screw-driven load frame demonstrating a tension test (left) and image of Instron 5982 load frame at AFRL/RWME (right)

2.3 Preliminary Mechanical Characterization Results

All experiments were conducted under identical conditions – the prescribed nominal engineering strain rate was 5 x 10^{-3} s^{-1} and all samples were tested to failure. All samples were Los Alamos national Laboratory (LANL) circular cross-section dogbones which have nominal gauge section dimensions of 25 mm height and 12.7 mm diameter. Deformation (strain) in the samples was

calculated based on crosshead displacement, which is typically not recommended, however the materials under consideration in this work have failure stresses less than 1% of the maximum load capacity of the load frame (100 kN), thus load frame deformation is negligible. The stress in the sample was calculated from force measurements made with a 1 kN load cell. Both stress and strain are reported as engineering values, where no assumption has been made about volume conservation.

Figure 5 shows the engineering stress vs. strain curve for one of the composites which has a 45% solids loading (by volume) of 22 micron glass beads. Figures 6-8 show how the elastic modulus, tensile strength and ductility respectively, vary with particle size and solids loading. From these figures, we see that for the composites tested the properties for a given particle mass fraction are effectively the same, since both average points lie within the uncertainty bars. As solids loading increases, the elastic modulus increases in a linear fashion for both particle sizes. The tensile strength appears to be fairly independent of solids loading however the ductility decreases with increasing solids loading.

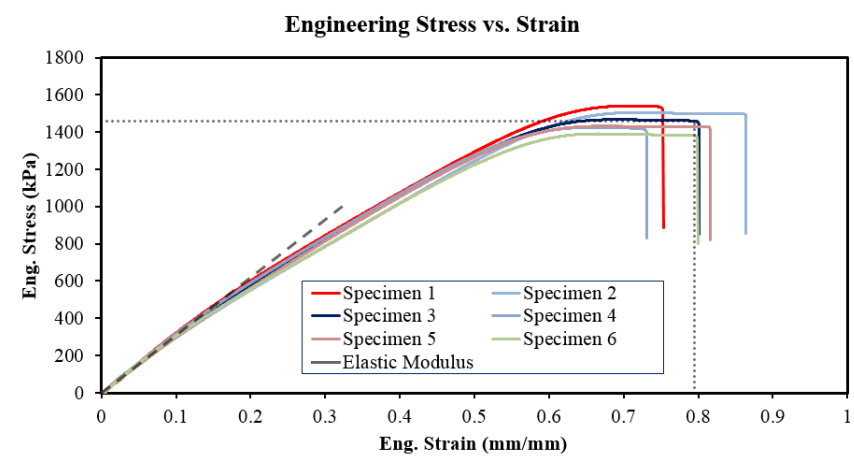

Figure 5. Stress-strain curve for 45% solids loading composite with 22 micron glass beads

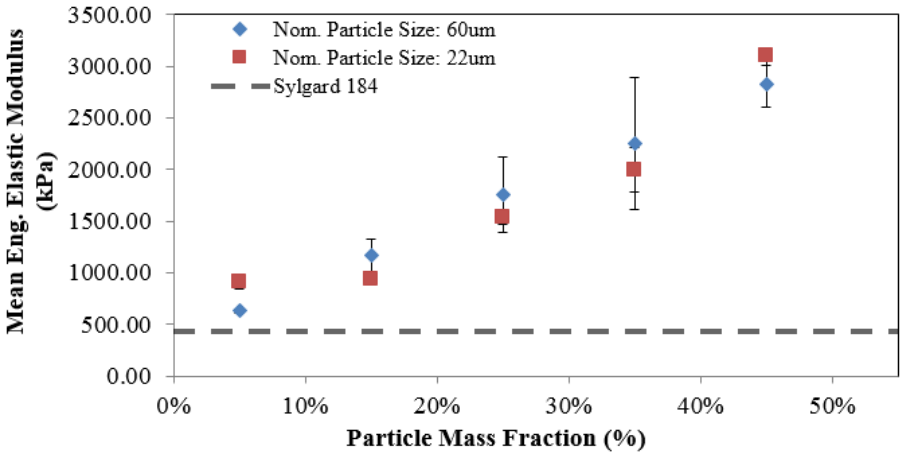

Figure 6. Elastic modulus as function of solids loading

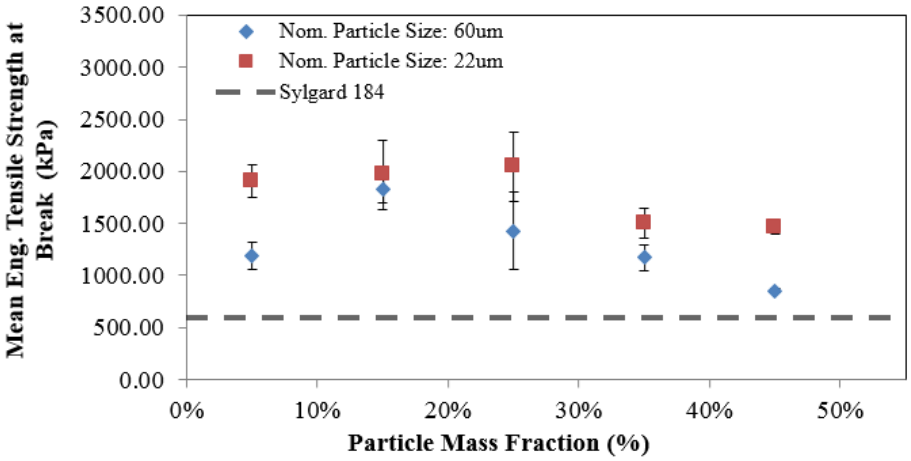

Figure 7. Tensile strength as function of solids loading

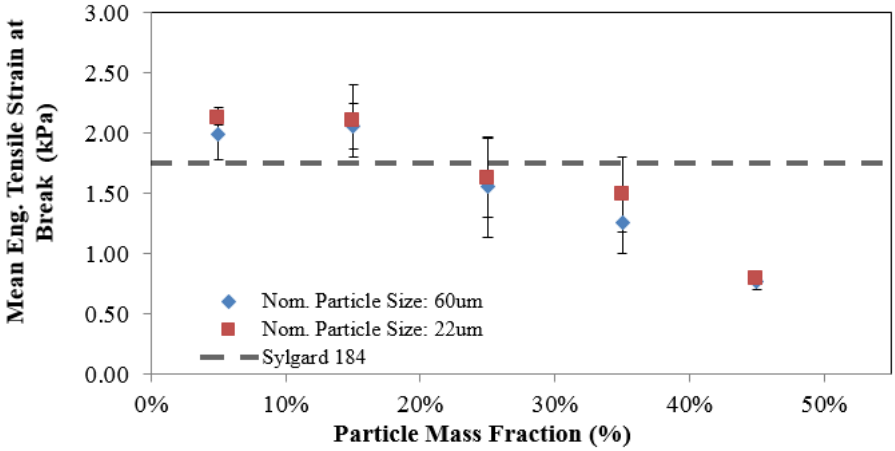

Figure 8. Ductility as function of solids loading

2.4 Plans for FY18

Research plans for FY18 Mechanical Properties Characterization include:

- Complete bulk composite characterization of Sylgard/glass bead composites
- Characterize interface using single-particle Sylgard/glass bead composite with Digital Image Correlation as diagnostic for 2D strain field
- Begin correlating mechanical properties with measured work of adhesion

3 Modeling and Simulation

3.1 Microstructure Characterization

Our team leveraged work by Dr. Chris Molek's Lab Task team in microstructural characterization and collaborated with them to develop new methods of quantitative image analysis for SEM images of microstructures. These sections of this report are therefore representative of that collaboration, and some duplication of content should be expected between the two annual reports.

3.1.1 Image Segmentation

Current methods of the segmentation of the SEM images are based on the grayscale intensity of individual pixels. The histogram of the grayscale values are fit with a bi-modal distribution to determine the mean intensity levels representing the void space and material. A threshold level is selected as a set multiple of standard deviations below the mean grayscale level representative of the material. Individual, fully-connected regions are then identified as separate instances of void and material. An illustration of this segmentation process is presented in Figure 9. Shape metrics are then calculated for each individual instance and statistics can be gathered. Future work will extend the current segmentation techniques to account for multiple constituent materials within a composite (i.e. binder, particle, void). The current simple grayscale threshold technique is not well equipped to separate the binder material from the particles, as found for preliminary images of pressed binderized composite materials. Techniques, including local pattern based analysis, will be integrated to achieve full and accurate segmentation of these composites as illustrated in Figure 10.

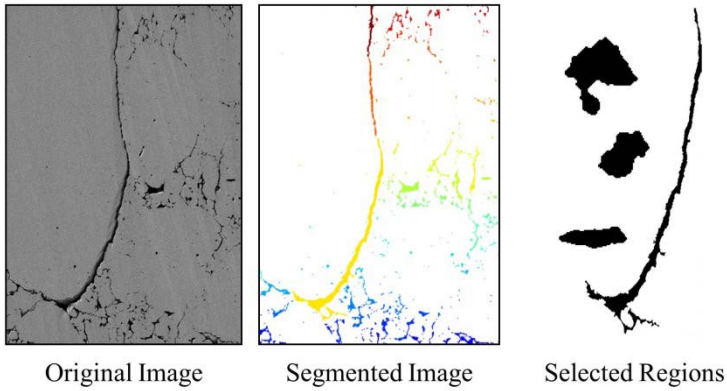

Figure 9. Left) Original image of a polished surface of a cross-sectioned pressed material taken via FIB-SEM. Center) Image illustrating individual (non-connected) regions of voids; each color represents a different void structure. Right) Selected examples of individual void structures extracted from the original microstructure image.

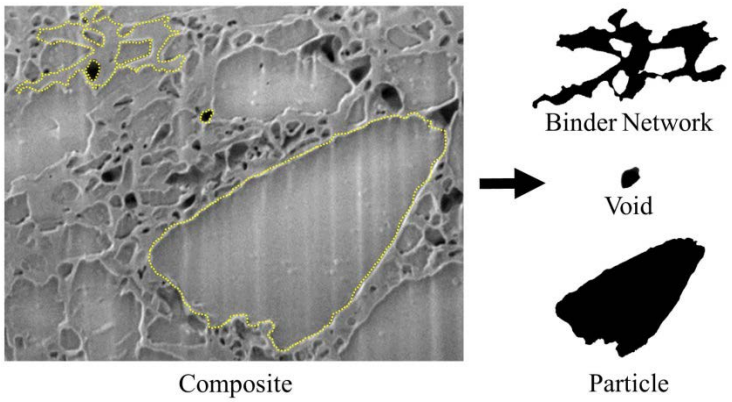

Figure 10. Left) Image of a polished surface of a cross-section pressed binderized composite taken via FIB-SEM. Highlighted regions indicate examples of different constituents within the composite. Right) Selected examples of individual structures extracted from the microstructure image

3.1.2 Shape Characterization

Basic shape metrics (area, perimeter, aspect ratio, etc.) were calculated for each individual region. It should be noted that the reported shape metrics are estimates of the true values of the regions due to the nature of the rasterized representation of the microstructure; the accuracy of these estimates are directly linked to the resolution limit of the imaging capabilities of the FIB-SEM. The basic shape metrics and the methods of implementation used in this work are given in Table 1.

More advanced shape metrics were implemented to more fully describe the structures of the regions; however, it was found that these metrics were only suitable for certain types of regions. Specifically, complex Fourier shape descriptors were successfully used to capture curvature detail of the contours of particles and spherical voids, or “pores”; however, this method failed to capture significant detail of the complex binder or crack networks. To more fully characterize the binder and crack networks, each region was deconstructed into separate “branches”, where more rudimentary metrics could then be employed. For this work, pores are geometrically defined as void shapes such that the circularity was greater than or equal to 0.65, solidity was greater than 0.30, and the bounding box aspect ratio was less than 7. This geometric threshold of the void shapes ensured that a distinction was made between “spherical” shaped void structures and more complex crack networks.

Table 1. Summary of definitions for current basic shape metrics

Shape Metric	Definition
Area	number of pixels in region
perimeter	sum of the distance between the mid-points of the outer most connected pixels
aspect ratio	aspect ratio of the minimum area bounding box surrounding the region
Angle	angle of the minimum area bounding box with respect to the image
centroid	location of the center of mass of the region with respect to the image
solidity	ratio of area of the void to the area of the bounding box
circularity	ratio of perimeter of an area-equivalent circle to the perimeter of the region

3.1.3 Particle/Void Metrics

Complex Fourier shape descriptors [XR1, XR2] are used to fully characterize the contour of the regions representing particles and pore shapes.[26-27] This technique requires that the x- and y-distance from the shape centroid to the contour is parameterized along the normalized path length of the contour, as shown in Figure 11. These functions are then sampled at equi-spaced intervals along the normalized path length and it should be noted that for any closed contour, these functions are cyclic on the interval 0 to 1. For convenience, these two functions are then represented on the real and imaginary plane as single complex values as a function of the parameterized path. The spatial frequency content of this complex valued function is obtained through a discrete Fourier transform, and the resultant real and imaginary spectra (Figure 12) are valuable in interpreting the spatial variations of the contour.

The lower order harmonics of the resulting spectra are associated with the “bulk” form of the contour shape, whereas the higher order harmonics represent the finer spatial details such as “roughness”. As such, the “surface roughness” of the particle or pore shapes can be quantitatively characterized via this technique. It is expected that the surface roughness and spatial variation along the particle boundaries heavily influence the total interface strength between the binder and particle. Furthermore, it is expected that large amplitude variations on the smaller spatial scale along the particle surface may indicate regions where localized stress concentrations may occur under various loading conditions. These surface features would play a key role in determining the likelihood of fracture and delamination within a composite material. These features are important to examine and may increase our understanding of the role of the surface modifiers in affecting delamination at critical stress locations within a composite material.

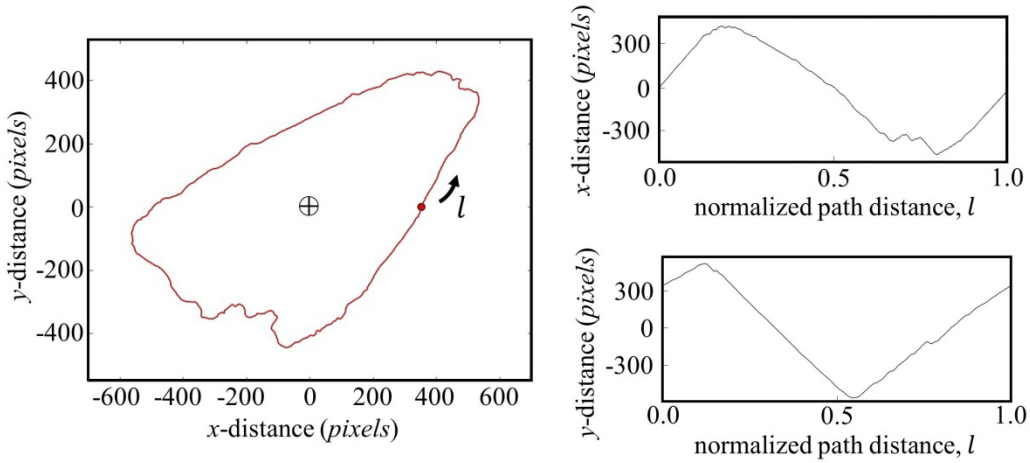

Figure 11. The contour of a selected pore shape as defined on an x,y-plane with respect to the centroid. The x- and y-values of the contour are parameterized as a function along the normalized path length, l.

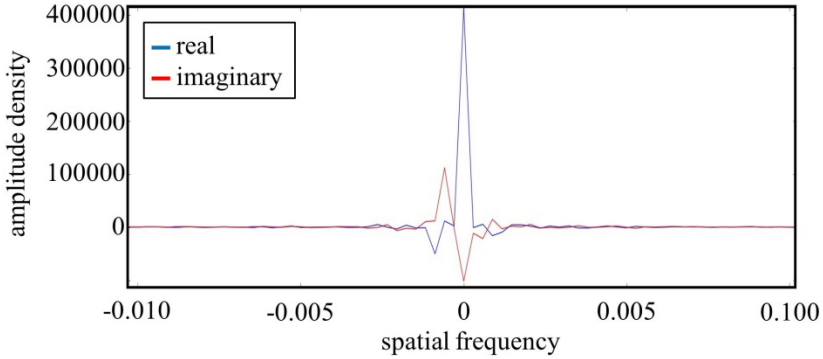

Figure 12. The spatial frequency content of the selected pore shape presented in Fig. X-3. The lower order harmonics are near the 0 location of x-axis.

3.1.4 Binder/Crack Network Metrics

The regions which represent the binder/crack networks were found to be unsuitable for characterization via complex Fourier shape descriptors, due to the highly complicated definition of the shape contour. Instead, these networks are analyzed by deconstructing each network as a connected set of individual branches and branch points. An example of a crack network, and its set of individual branches, is presented in Figure 13. The set of branches are established via a skeletonization algorithm performed on the selected binder or crack network and joints are defined at locations where the skeleton bisects, or ends. The branches are then defined as the network skeleton between these defined joints.

These branches are then characterized via simple metrics such as thickness, angle, and length. Specifically, the thickness of the branch is specified as the distance from each pixel along the branch to the nearest contour of the crack network, such that the branch thickness is a function of distance along the branch. These metrics are then summarized in terms of the totals, medians, and

means, such that the entire crack network can be represented by the median crack thickness, total crack length, number of branches, etc.

It is expected that these characteristics of the binder/crack networks are crucial in understanding the effects of bulk mechanical properties of the composite system. For example, the binder thickness between particles may be extremely important to examine the effect of the surface modifiers on the nearby binder material. With this understanding we may begin to gain insight into the effective length of the transition zone between the binder and particle material. Additionally, the orientations of the crack/ binder networks are expected to affect the fracture and delamination behavior, specifically if there is an overall preferential orientation caused by pressing or casting methods.

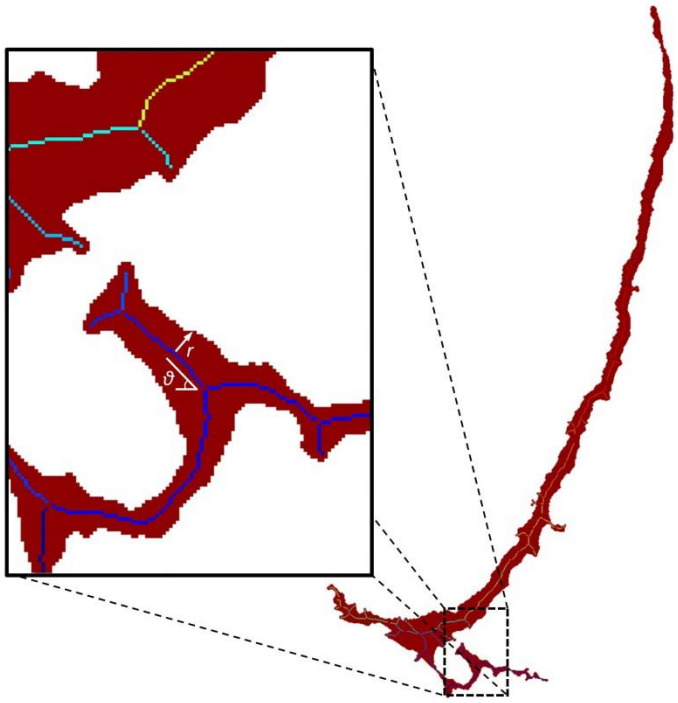

Figure 13. A complex crack network as represented by the red-shaded region. Individual branches are represented by different colors as shown in the inlay. Each branch is characterized by simple metrics such as branch angle and branch thickness as a function of travel distance along the branch.

3.1.5 Spatial Distribution Metrics

To account for the spatial distribution of particle and features within the composite materials, specific metric have been developed for image analysis. Euclidean distance maps have been implemented to quantify distances between certain features, such as void space or cracks, as shown in Figure . These metrics are useful in determining physical distribution of materials within the composite structure, which are unable to be captured by the mass or volume fraction alone. Furthermore, these metrics may be useful in evaluating the effect of surface modifications on the effective dispersion of materials. In addition to the Euclidian distance analysis, a more recently developed metric known as “lacunarity” has been implemented to investigate the level of spatial “clumping” of feature within a composite material.[28] This metric has been proposed to indicate levels of heterogeneity vs. homogeneity as a function of length scales of interest over an image

when referenced to a Brownian process.[29] An example of this metric as a function of the length scale for an image of pressed HMX is presented in Figure 15. This metric may provide a basis in determining suitable length scales for representative volumetric elements used in micromechanics simulation efforts to predict the mechanical response of these materials to various loading regimes.

Fractal analysis methods have also been implemented for image analysis to account for the spatial distribution of materials within the microstructure with respect to various length scales of interest. The fractal dimension was calculated using a box-counting method.[30] An example result of fractal analysis on the microstructure of a pressed sample of HMX is given in Figure 16. It has been proposed that fractal analysis in explosive materials may be suitable to quantify traditional damage to these materials.[31] This method would therefore allow for the study of the effect of interface adhesion on the ability to mitigate damage.

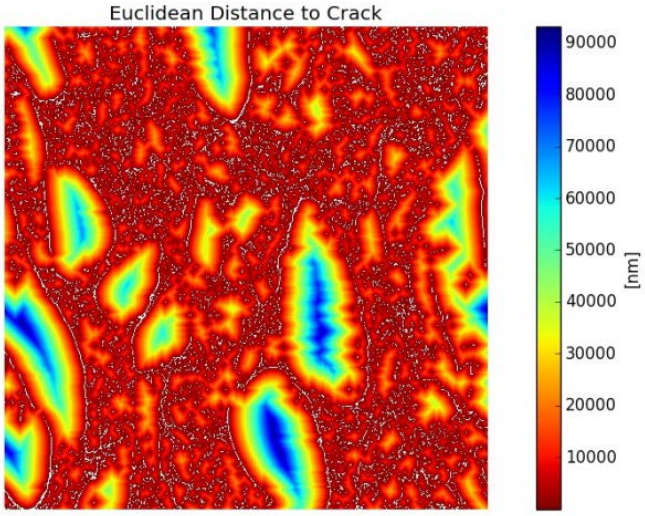

Figure 14. A map of the Euclidean distance to a crack feature within a pressed sample of HMX

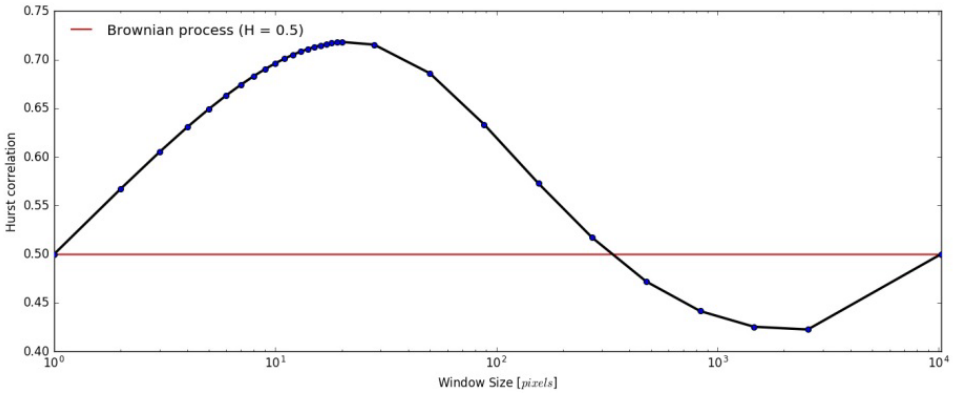

Figure 15. An image showing the lacunarity index of an image of a pressed HMX sample, taken with respect to a Brownian process as a function of the window size, or length scale. In this example, the metric indicates a large level of heterogeneity at small length scales and shifts to a more homogeneous representation of the image at larger window sizes.

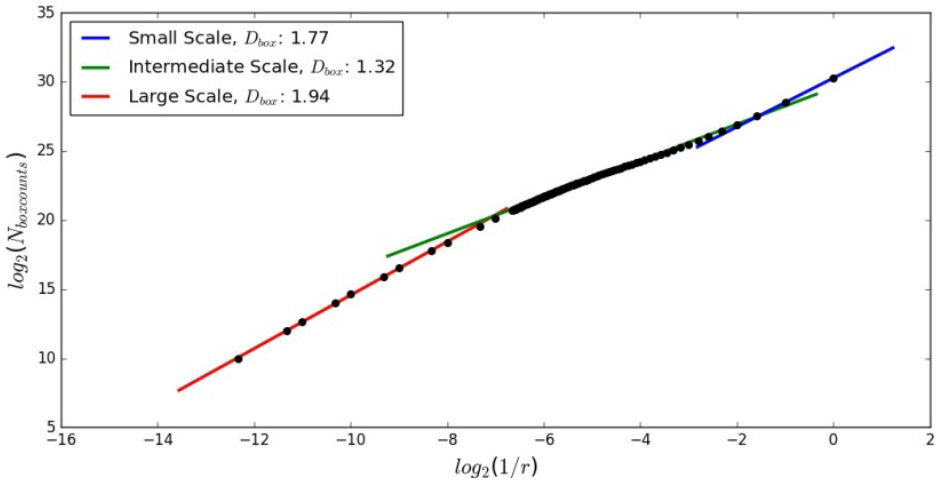

Figure 16. An image illustrating the fractal dimension of an image of pressed HMX sample. The fractal dimension was calculated using a box-counting method and the relationship of the number of boxes to the length scale is demonstrated as three separate linear regions. These upper and lower regions are expected to be due to the limitation of the resolution of the SEM and the limitation of field of view of the image.

3.1.6 Statistical Representation

These metrics are collected for every appropriate region within an image and are combined with the corresponding results from multiple images of a single sample. In this manner, a statistical representation of a sample in terms of each of these selected metrics can be constructed. For preliminary samples of pressed HMX, it has been found that many of the basic metrics follow a log-normal distribution, as show in Figure 17. It is expected that many of these metric can thus be effectively represented by common distribution functions allowing for data reduction and quantitative comparisons between samples.

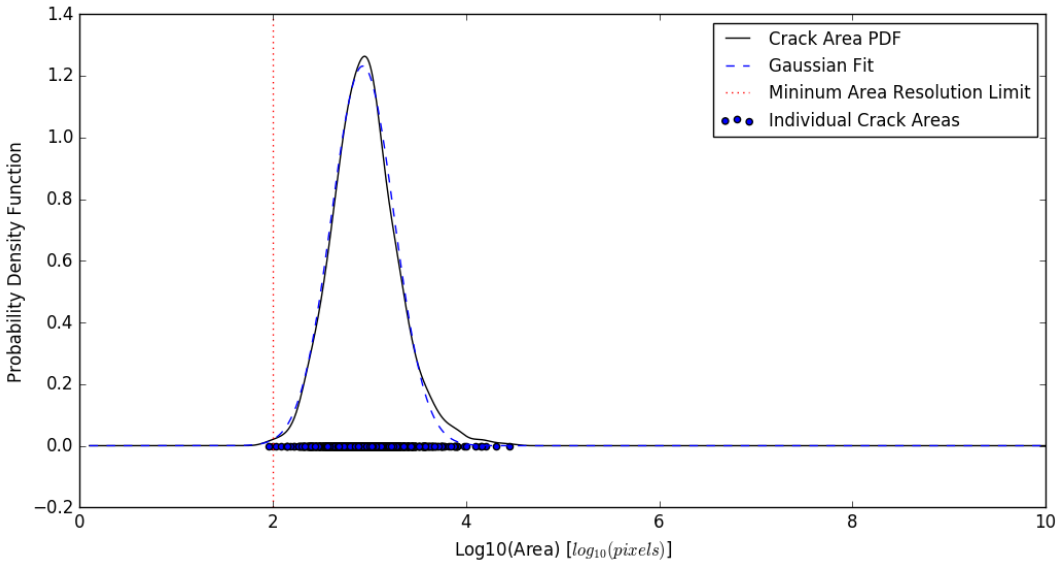

Figure 17. A distribution of the areas of the cracks measured within an SEM image of pressed HMX. The distribution appears to closely follow a fitted log-normal distribution, indicating that the metric can be well represented by a measured mean and standard deviation.

3.2 Interface Modeling Techniques

3.2.1 Interface representation

To model the effect of interfaces on the overall mechanical behavior of materials, it is necessary to accurately model the behavior of the interface itself as well as any nearby material that may behave significantly different than the bulk material of the same type. To that end, we will employ two different types of models to describe the process of debonding and damage in the vicinity of the interfaces: cohesive zone elements to explicitly model a zero thickness interface and continuum damage elements to model a finite thickness band of modified, damageable material that makes up the interface (or interphase region).

3.2.1.1 Cohesive zone elements

Finite elements utilizing a cohesive zone method are used to model a zero thickness interface which deforms and eventually fails due to constitutive laws. For this class of elements, the constitutive equations are written in the form of a so-called traction-separation law which relates the relative displacement of the two sides of an element (separation) to the stress carried across the interface (traction). Figure 18 provides a practical illustration of the behavior of a bilinear traction separation law subjected to a complicated load path. The initial loading from A to B is purely elastic deformation through previously undamaged material. At point B, the material reaches its maximum traction, and damage begins to accumulate with increasing separation from B to P. Next, the material is unloads from P to A along a modulus that has been degraded by the induced damage. However, in this model when the load is fully removed, the material returns to its undeformed position (point A in this graphic). The material is elastically reloaded from A to P, the material's stiffness has been degraded by prior damage and the new maximum traction is P. Finally, when the material is loaded to C, it is fully damaged and a new surface is created on each side of the cohesive element.

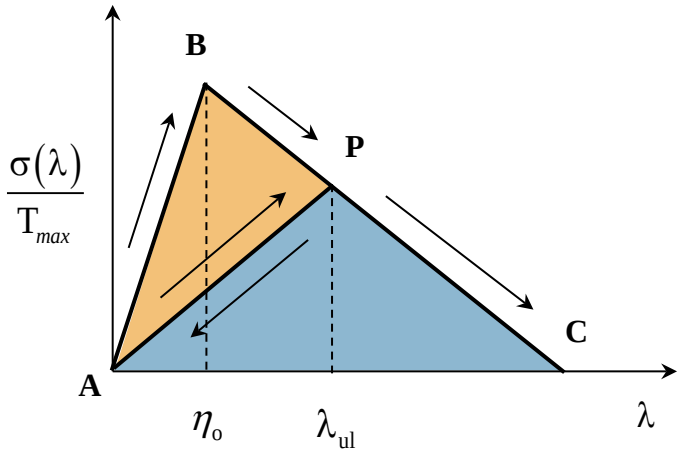

Figure 18. Pictoral description of a bi-linear traction-separation constitutive law where λ is the separation (in tension or shear) of the two faces of a cohesive element and σ is the traction on the interface for a given separation.

The cohesive zone model to be used is described by Equations 7-9 below. The monotonically increasing, accumulated damage parameter is calculated as

$$\lambda = \sqrt{\left(\frac{\Delta_n}{\Delta_{nc}}\right)^2 + \left(\frac{\Delta_t}{\Delta_{tc}}\right)^2}. \tag{7}$$

where Δ_n and Δ_t are the normal and tangential components of the separation, respectively and Δ_{nc} and Δ_{tc} are the critical normal and tangential separations at failure, respectively. The generalized traction on the interface is then given by

$$\sigma = \sqrt{\left(T_n\right)^2 + \left(\frac{T_t}{\alpha}\right)^2} = \begin{cases} \left(T_{max}\frac{1-\eta}{1-\eta_0}\right)\frac{\lambda}{\eta}, & \text{if } 0 \le \lambda \le \eta; \\ \left(T_{max}\frac{1-\eta}{1-\eta_0}\right)\frac{1-\lambda}{1-\eta}, & \text{if } \eta < \lambda \le 1; \\ 0, & \text{if } \lambda > 1. \end{cases} \tag{8}$$

where T_n and T_t are the normal and tangential tractions, T_{max} is the maximum traction, and η is the history dependent measure of separation.

$$T_n = \sigma(\lambda,\eta)\frac{\Delta_n}{\lambda\Delta_{nc}} \quad \text{and} \quad T_t = \sigma(\lambda,\eta)\frac{\alpha\Delta_t}{\lambda\Delta_{tc}}; \quad \alpha = \frac{\Delta_{nc}}{\Delta_{tc}}. \tag{9}$$

3.2.1.2 Continuum damage elements

One major assumption in the usage of cohesive elements is that the damage and failure occur precisely on the interface which separates two adjacent materials. This assumption is in direct opposition to a number of experimental observations of failure in the vicinity of small spherical inclusions. These experiments show that surface debonding is the dominant failure mechanism for

large particles, but that the location of the failure moves away from the interface as the particle size decreases. In an effort to capture this phenomenon, we will model the region around an inclusion with a continuum damage model. This model includes the introduction of a damage parameter, D, which monotonically increases from 0 (pristine, undamaged) to 1 (fully damaged). This modifies the stress in the damaged material according to

$$\boldsymbol{\sigma} = (1 - \mathrm{D})\overline{\boldsymbol{\sigma}} \tag{4}$$

where $\overline{\boldsymbol{\sigma}}$ is the effective stress calculated as if the material were undamaged and $\boldsymbol{\sigma}$ is the stress carried by the damaged material. When D = 1, the material is fully damaged and has lost all load carrying capability. In this model, damage initiation is controlled by a specific damage criterion that can be a function of stress, strain, strain rate, temperature, etc. Once initiated, a damage evolution law controls the progress of damage from 0 to 1. This type of model makes it possible to capture the effect of changing location of failure as a function of inclusion size and binder material.

3.2.2 Computational Domain(s) for Interface Investigation

For each of the interface modeling approaches, we will be looking at two distinct types of computational domains for investigating interface effects: a unit cell approach and an approach utilizing representative volume elements (RVEs). The domain types are summarized in the following subsections including descriptions of the particular domains to be used as well as the motivation for pursuing each domain type.

3.2.2.1 Unit cell calculations

The first calculations to be performed are the unit cell calculations. The goal of this type of calculation is to probe the effects of differences in interface properties in a number of simple geometries which allows for separation of some of the more complex geometrical effects that will play a significant role in both real specimens and in the RVE calculations discussed below. Because this scale of calculation allows us to focus specifically on the role of the interface with a minimal number of confounding variables. For this phase of the Lab Task, we will be looking at three different unit cells: a round inclusion in a field of binder, two particles with a single flat interface with binder, and a triple point of 3 particles with flat binder interfaces connecting them. These unit cells are shown in Figure 9, Figure, and Figure. These domains can be subjected to a number of applicable loading conditions to probe the interfacial behaviors, but for this work they will be minimally exposed to both a uniaxial tensile load and a pure shear load.

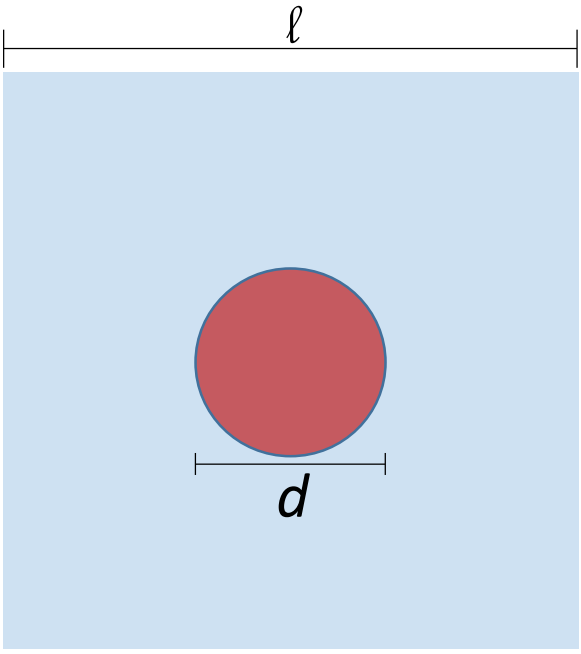

Figure 19. Simple unit cell domain containing a single circular (spherical) particle embedded in a polymer field. The two parameters which describe this domain are the particle diameter, d, and the characteristic specimen size, l.

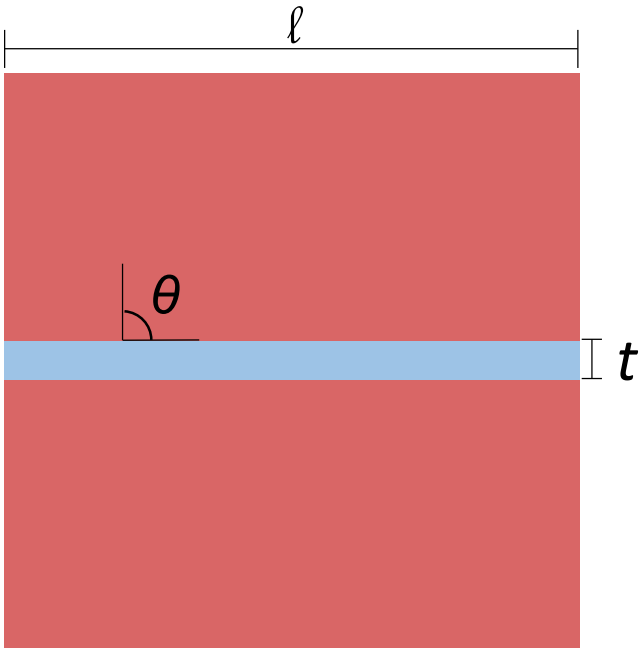

Figure 20. Simple unit cell domain containing a single, planar binder region connecting two particles. The parameters describing this domain are the characteristic specimen size, l, the thickness of the binder region, t, and the orientation of the binder region relative to the loading direction, θ.

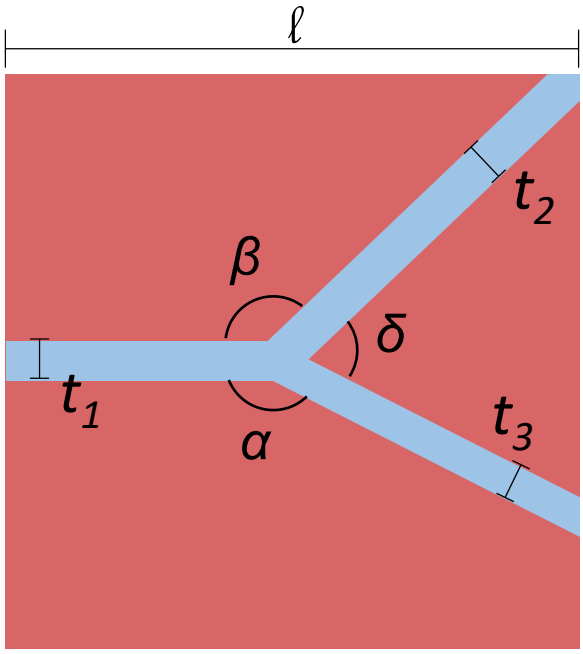

Figure 21. Simple unit cell domain containing a triple-point junction of three particles. The parameters which fully determine this domain are the angles (α, β, and δ), the binder thicknesses (t_1, t_2, t_3), and the characteristic specimen size (l).

3.2.2.2 RVEs

Due to the high volume fraction of inclusions in typical energetic composites of interest, it is necessary to develop a capability of characterizing the effect of these microstructures in relevant microstructures with a statistically significant domain size. The domain(s) for these calculations should meet one of two criteria: 1) a single domain should be large enough that there is very little variation in the predicted response due to reorganization of the particles or 2) sufficient number of domains such that the response of a future domain from the same material can be predicted from the results of the prior domains. A typical example of an RVE type of domain is shown in Figure 22 for both synthetic and real microstructures. The rationale behind performing simulations on RVEs rather than on the much less complex unit cells is that we will be able to capture (in a statistical sense) the effect of hard to disentangle effects such as the interaction of multiple particles, varying width of binder separating particles, and irregularly distributed particles, interfaces, and initial defects. In general, it is expected that this path contains the most potential for extending our understanding of interface property modification from the interface scale to the engineering property scale.

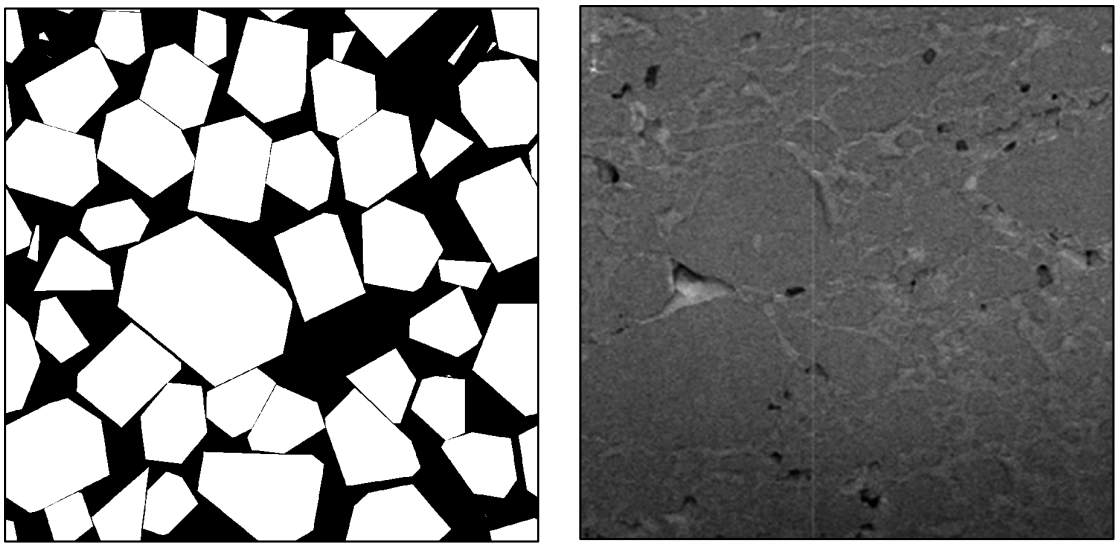

Figure 222. Two types of representative volume elements (RVEs) to be used are synthetic microstructures (left) and microstructures extracted from SEM images of actual composites of interest (right).

3.2.3 Linkage of Modeling to Experimental Results

In order to have confidence in the predictions and modeling ability of the unit cell and RVE calculations, the material models used to describe the binder and interface behavior should be tightly coupled with experimental results. To that end, we are using the tightly controlled, highly characterized experimental setup shown in **Error! Reference source not found.**23 to parameterize the mechanical response of both the binder and interfacial region. The experiment is simply the failure under uniaxial strain of a single glass bead suspended in a silicone binder. What makes this experiment most useful for coupling to computations is the ability to distribute aluminum powder (seen as white specks in **Error! Reference source not found.**) and use this powder for performing digital image correlation (DIC) on the centerline of the specimen. DIC analysis then provides a full plane measure of strain along the mid-plane of the specimen. We then use the global load – displacement curve measured from the test coupled with the DIC results to parameterize the constitutive behavior of both the binder and the interface through an iterative approach which minimizes the error between the observed experimental results and the modeled computational response. This approach is complimentary to an approach being pursued at Purdue within the group of Prof. Vikas Tomar.[32] Dr. Tomar's work experimentally measures the stress along an interface as it is being loaded to failure. The major limitation to the Purdue technique is that it is only able to measure stresses on the surface of a specimen. Because it is a surface technique, it would be insensitive to variations in behavior of the binder or interface as a function of distance from the surface. Our technique will be able to parameterize the same constitutive laws as Dr. Tomar's using internal measurements. We are working with their group to validate both approaches by comparing our predicted material properties at the surface, where our capabilities should converge to the same solution. The constitutive laws parameterized in this portion of the effort are then being used directly in the unit cell and RVE calculations to understand the effect of these interface properties on the bulk behavior of the composite systems.

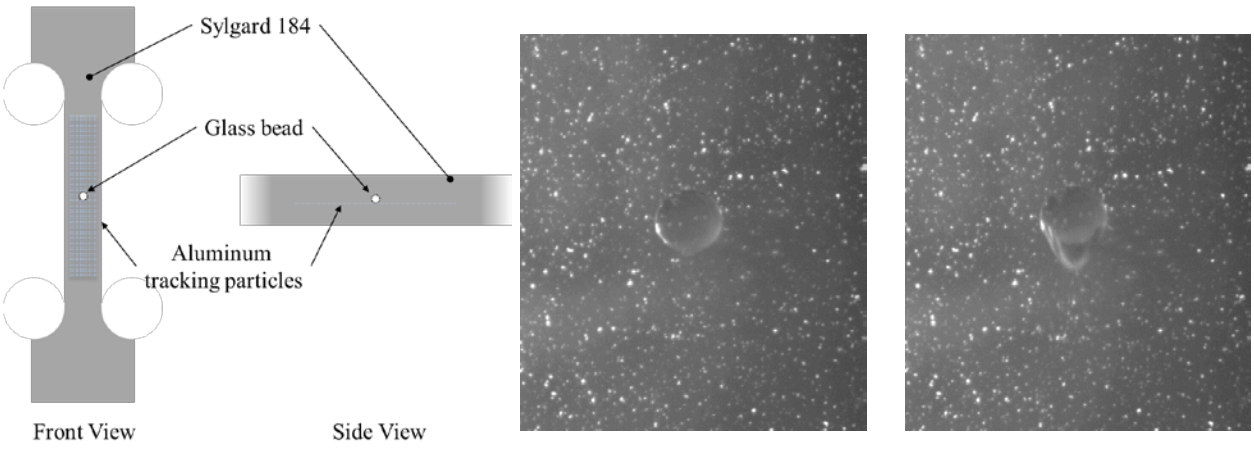

Figure 23. Experimental setup (left) of single glass bead in a silicon specimen. Aluminum powder is used as tracking particles and can be seen in the before failure (center) and immediately following failure (right) images. The glass bead can be seen debonding from the bottom, in line with the direction of loading.

3.3 Plans for FY18

Research plans for FY18 Modeling and Simulation include:

- Develop specific input-deck implementations for modeling of mechanical response for microstructures in ABAQUS – both for RVE volume elements and for unit cell volume elements;
- Automate microstructure-based modeling of the unit cell elements;
- Develop analysis tools to compare unit cell simulation results with RVE results;
- Exercise the tools developed to perform simulations of both RVEs and unit cells based upon microstructure images from Dr. Molek's Lab Task research, and compare results between the two approaches.

4 References:

1. Molek, C.D.; Fajardo, M.; Welle, E.J. *"Effects of microstructural properties on chemical energy release and initiation processes of energetic materials"*, AFOSR LRIR, work started **2015** at Eglin AFB.
2. Grajek, H.; Paciura-Zadrozna, J.; Witkiewicz, Z. *J. Chromatogr. A*, **2010**, *1217*, 3105.
3. Thielmann, F. *Characterization of Alumina and Other Inorganic Materials by Inverse Gas Chromatography*, Surface Measurement Systems, **2010**.
4. Grajek, H.; Paciura-Zadrozna, J.; Witkiewicz, Z. *J. Chromatogr. A*, **2010**, *1217*, 3116.
5. Gutmann, V. *The Donor-Acceptor Approach to Molecular Interactions*, Plenum Press, NY, **1978**.
6. Lara, J.; Schreiber, *J. Coat. Technol.*, **1991**, *63*, 81.
7. Papadopoulou, S.K.; Dritsas, G.; Karapanagiotis, I.; Zuburtikudis, I.; Panayiotou, C. *Eur. Polym. J.*, **2010**, *46*, 202.
8. Sengupta, A. and Schreiber, H.P. *J. Adhesion Sci. Technol*., **1991**, *5*, 947.
9. Zhao, S.; Song, J.; Wang, S. *Wood Sci. Technol.*, **2009**, *43*, 105.
10. Tisserand, C.; Calvet, R.; Patry, S.; Galet, L.; Dodds, J.A. *Powder Technol.*, **2009**, *190*, 53.
11. Panayiotou, C.G. *J. Chromatogr. A*, **2012**, *1251*, 194.
12. Glass, A.S.; Larsen, J.W. *Macromolecules*, **1993**, *26*, 6354.
13. Mohammadi-Jam, S.; Waters, K.E. *Adv. Colloid and Interface Sci.*, **2014**, *214*, 21.
14. Dorris, G.M.; Gray, D.G. *J. Colloid Interface Sci.*, **1980**, *77*, 353.
15. Schultz, J; Lavielle, L.; Matrin, C. *J. Adhesion*, **1987**, *23*, 45.
16. van Oss, C.; Good, R.; Chaudhury M. *Langmuir*, **1988,** *4*, 884.
17. Dong, S.; Brendle, M.; Donnet, J.B. *Chromatographia*, **1989**, *28*, 469.
18. Davies, M.; Brindley, A.; Chen, X.; Marlow, M.; Doughty. S.W.; Shrubb, I.; Roberts, C.J. *Pharm. Res.*, **2005**, *22*, 1158.
19. Della Volpe, C.; Siboni, S. *J. Colloid Interface Sci.*, **1997**, *195*, 121.
20. Luo, Y.; Du, M. *Prop. Expl. Pyro.*, **2007**, *32*, 496.
21. De Boer, J.H. *The Dynamic Character of Chemisorption*, Clarendon Press, Oxford, **1953**, 82.
22. Feeley, J.C.; York, P.; Sumby, B.S.; Dicks, H. *J. Mater. Sci.*, **2002**, *37*, 217.
23. Chehimi, M.M. *Surface Thermodynamics of Solid Materials by Inverse Gas Chromatography*, Springer, Paris, **1998**, 135.
24. *IGC Application Note 220*, Surface Measurement Systems, London, **2013**.
25. Internal AFRL/RWME Technical Memoradums.
26. Granlund G. H., "*Fourier preprocessing for hand print character recognition*", IEEE Transactions on Computers, **1971**.
27. Sjostrand *et al.*, "*On the alignment of shapes represented by Fourier descriptors*", Proc. SPIE Int. Soc. Optical Eng., **2006**.
28. Plotnick R.E *et al.*, "*Lacunarity indices as measures of landscape texture*", Landscape Ecology 8:33, **1993**.
29. Feagin R.A., "*Relationship of second-order lacunarity, Hurst exponent, Brownian motion, and pattern organization*", Physica A 328, **2003**.
30. Jiang S. and Liu D., "*Box-counting dimension of fractal urban form: stability issues and measurement design*", Int. J. Artificial Life Research, 3(*3*), **2012**.

31. Chen P. *et al.*, "*Detection and characterization of long-pulse low-velocity impact damage in plastic bonded explosives*", Int. J. Impact Eng., 31, **2005**.
32. Gan, Ming, and Vikas Tomar. *"An in situ platform for the investigation of Raman shift in micro-scale silicon structures as a function of mechanical stress and temperature increase."* Review of Scientific Instruments 85.1 (**2014**): 013902.

Appendix: In-house Activities

Personnel:	Name	Degree/Discipline	Involvement
Air Force Employees:			
	Stacy M. Manni	Ph.D. Chemistry	50%
	Stephen Pemberton	Ph.D. Mechanical Engineering	25%
	Barrett Hardin	Ph.D. Mechanical Engineering	20%
	Tomislav Kosta	M.S. Mechanical Engineering	15%
	Lindsey Cromwell	B.S. Industrial Engineering	10%
On Site Contractors:			
	Murphy Mitchell	N/A	100%
	Jesus Mares	Ph.D. Mechanical Engineering	10%

Visitors:
- N/A

Collaborations:
- Vikas Tomar (Purdue)
- Caglar Oskay (Vanderbilt)
- Andrew Guenthner, Joseph Mabry, Joseph Mates and Kamran Ghiassi (AFRL/RQR)
- Hilmar Koerner and Timothy Pruyn (AFRL/RXC)

Publications:
- N/A

Invited Presentations:
- N/A

Invention Disclosures and Patents Granted:
- N/A

Professional Activities:
- N/A

Honors and Awards Received:
- N/A

Extended Scientific Visits:
- N/A

Technology Transitions:
- N/A

DISTRIBUTION LIST

AFRL-RW-EG-TR-2018-098

*Defense Technical Info Center
8725 John J. Kingman Rd Ste 0944
Fort Belvoir VA 22060-6218

AFRL/RWME (1)
AFRL/RWORR (STINFO Office) (1)